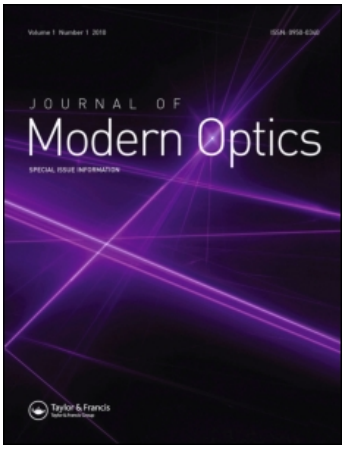

Journal of Modern Optics
Publication details, including instructions for authors and subscription information:
http://www.informaworld.com/smpp/title~content=t713191304

Light trapping in high-density ultracold atomic gases for quantum memory applications

I. M. Sokolov[ab]; D. V. Kupriyanov[a]; R. G. Olave[c]; M. D. Havey[c]
[a] Department of Theoretical Physics, State Polytechnic University, 195251 St. Petersburg, Russia [b] Institute for Analytical Instrumentation, Russian Academy of Sciences, 198103 St. Petersburg, Russia [c] Department of Physics, Old Dominion University, Norfolk, VA 23529, USA

First published on: 02 July 2010

To cite this Article Sokolov, I. M. , Kupriyanov, D. V. , Olave, R. G. and Havey, M. D.(2010) 'Light trapping in high-density ultracold atomic gases for quantum memory applications', Journal of Modern Optics, 57: 19, 1833 — 1840, First published on: 02 July 2010 (iFirst)
To link to this Article: DOI: 10.1080/09500340.2010.493977
URL: http://dx.doi.org/10.1080/09500340.2010.493977

Journal of Modern Optics
Vol. 57, No. 19, 10 November 2010, 1833–1840

Taylor & Francis
Taylor & Francis Group

Light trapping in high-density ultracold atomic gases for quantum memory applications

I.M. Sokolov[a,b]*, D.V. Kupriyanov[a], R.G. Olave[c] and M.D. Havey[c]

[a]*Department of Theoretical Physics, State Polytechnic University, 195251 St. Petersburg Russia;*
[b]*Institute for Analytical Instrumentation, Russian Academy of Sciences, 198103 St. Petersburg, Russia;*
[c]*Department of Physics, Old Dominion University, Norfolk, VA 23529, USA*

(*Received 24 February 2010; final version received 13 May 2010*)

High-density and ultracold atomic gases have emerged as promising media for storage of individual photons for quantum memory applications. In this paper we provide an overview of our theoretical and experimental efforts in this direction, with particular attention paid to manipulation of light storage (a) through complex recurrent optical scattering processes in very high density gases (b) by an external control field in a characteristic electromagnetically induced transparency configuration.

Keywords: quantum information; quantum memories; light localization; electromagnetically induced transparency; coherent multiple scattering

1. Introduction

Manipulation of photonic degrees of freedom plays an important role in many aspects of quantum information sciences [1]. One of these is the storage of photonic information via a quantum memory, which forms an essential element of an optical quantum repeater [2]. One candidate for such a memory is an ultracold atomic gas [3], which can have such desirable qualities as very narrow and thus selectable resonance response, relative ease of manipulation of the atomic density, and precise control of many aspects of the atomic physical environment [4,5]. Long-lived atomic coherence may readily be generated, facilitating the formation, in lower density gases, of dark state polaritonic excitations using, for example, an optical Λ configuration [6–9]. Various environmental factors limit the lifetime of these coherences, and hence the time-scale of efficient optical storage in the medium. An additional important factor that can limit the atomic coherence is multiple light scattering of near-resonance radiation in an optically thick atomic ensemble [10]. Multiple light scattering in atomic gases is quasi-elastic, and so the scattered light can remain in a coherent state. This situation corresponds in the lower density case to the so-called weak localization regime, where such scattering can produce macroscopic observables such as the coherent backscattering cone [11–22]. The weak localization case is characterized by the inequality $kl \gg 1$, where $k = 2\pi/\lambda$ is the light wave vector, and l is the mean-free path for light scattering. Such an effect promises to help clarify the role of multiple light scattering for quantum memory applications in this case. For much higher atomic densities, such that $kl \sim 1$, light scattering enters the so-called strong localization regime. In this case, recurrent light scattering can lead to formation of long-lived atomic–photonic excitations which are currently under investigation as possible quantum memories, in searches for Anderson localization of light [23–27], development of atomic-physics based random lasers [28,29], and for studies of single and multiple photon cooperative scattering [30–33].

In this paper we provide a brief overview of our theoretical and experimental light storage programs using as approaches either light localization or electromagnetically induced transparency. This is accompanied by new results in several areas which illustrate some of the factors important in the physical processes. We concentrate particularly on the influence of multiple scattering in ultracold clouds, and its role in the time-scale associated with quantum information storage.

2. Light storage and light localization

2.1. Introduction

We have recently reported a comprehensive description of our theoretical approach to treatment of light scattering in very high density and ultracold atomic gases [34]. The atomic density used in these calculations corresponds closely to the Ioffe–Regel condition for light localization. In [34] we used two different but

*Corresponding author. Email: ims@isi2093.spb.edu

ISSN 0950–0340 print/ISSN 1362–3044 online

DOI: 10.1080/09500340.2010.493977
http://www.informaworld.com

complementary approaches. In the first, we employed a self-consistent description of the atomic sample in the spirit of the Debye–Mie model for a macroscopic spherical scatterer consisting of a dense configuration of atomic dipoles. In the second, we take a microscopic approach in order to make exact numerical analysis of the quantum-posed description of the single photon scattering problem.

In the microscopic approach, the total scattering cross-section can be determined by the T-matrix, which in turn can be expressed by the total Hamiltonian $H = H_0 + V$ of the joint atomic–field system and by its interaction part V as $T(E) = V + V(E-H)^{-1}V$. In the rotating wave approximation the internal resolvent operator $(E-H)^{-1}$ contributes to $T(E)$ only by being projected on the states consisting of single atom excitation, distributed over the ensemble, and the vacuum state for all the field modes. Defining such a projector as P the projected resolvent $\tilde{R}(E) = P(E-H)^{-1}P$ performs a finite matrix of size determined by the number of atoms N and the structure of the atomic levels. For the considered $F=0 \leftrightarrow F'=1$ transition $\tilde{R}(E)$ is a $3N \times 3N$ matrix.

For a dipole-type interaction between atoms and field, the resolvent $\tilde{R}(E)$ can be found as the inverse matrix of the following operator $\tilde{R}^{-1}(E) = P(E - H_0 - VQ(E-H_0)^{-1}QV)P$, where the complementary projector $Q = 1 - P$, operating in the self-energy term, can generate only two types of intermediate states: a single photon plus all the atoms in the ground state; and a single photon plus two different atoms in the excited state and others are in the ground level. For such particular projections there is the following important constraint on the interaction Hamiltonian: $PVP = QVQ = 0$, which is apparently valid for a dipole-type interaction $V = -\Sigma \boldsymbol{d}_j \boldsymbol{E}_j$, where $\boldsymbol{d}_j$ is a dipole operator of the jth atom and $\boldsymbol{E}_j$ is the microscopic displacement field at the point where the atom is located. Due to this constraint the series for the inverse resolvent operator $\tilde{R}^{-1}(E)$ is expressed by a finite number of terms and an explicit analytical expression for $\tilde{R}^{-1}(E)$ is obtained, see [35,36] and Appendix B in [34]. The resolvent $\tilde{R}(E)$ and T-matrix can be calculated numerically for an atomic system consisting of several thousands of atoms. Thus, the microscopic approach gives us the exact value of the scattering amplitude for macroscopic atomic ensembles. Note that the described approach is similar to that used before [37,38] but in contrast to those discussions based on the scalar model, we make our calculations paying attention to the vector structure of the light and the atom–field interaction.

In this section, we present further elaboration of theoretical results obtained in [34], with particular emphasis on the spectral response of the total scattering cross-section, and the time evolution of the total light scattered from a spherical and high density sample, because such evolution is strongly connected with light trapping in the cloud. We have made all calculations in the framework of the vector model. At the end of this section we compare the vector and scalar approaches as applied to the microscopic scattering problem. These results show clearly that the frequently-used scalar model fails in a significant way for higher atomic densities $\sim 5 \times 10^{13}$ atoms cm^{-3}.

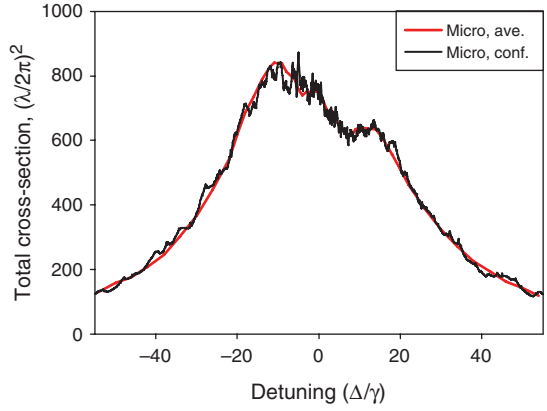

Figure 1. The spectral dependence of the total cross-sections for atomic samples of size $5(\lambda/2\pi)$ and density $n = 0.5$, made using the vector model. Calculations of the microscopic response for a particular configuration (black curve) indicates a micro-cavity structure generated by interatomic interactions in dense disordered media. (The color version of this figure is included in the online version of the journal.)

In this work, our theoretical discussion of time-dependent scattering is based on the microscopic approach. The knowledge of the resolvent operator $\tilde{R}(E)$ allows us to describe the interaction of the atomic ensemble with weak coherent light, which can be approximated as a superposition of the vacuum and single excitation states. Thus, considering the light pulse as a superposition of such coherent components, we generalize our approach to the case of non-steady state.

2.2. *Theoretical results*

We first present in Figure 1 the spectral variation of the total light scattering cross-section from a dense spherical cloud of ultracold atoms. For these calculations the sample radius is $10(\lambda/2\pi)$ and the atom density $n = n_0(\lambda/2\pi)^3 = 0.5$. As we mainly focus on our program on experiments with atomic Rb, $(\lambda/2\pi) = 780/2\pi$ nm, and the base unit of atomic density $(n=1)$ corresponds to 5.2×10^{14} atoms cm^{-3}. There are two results shown. The first corresponds to the scattering cross-section for a single realization of the atomic sample. This means that there is a single

configuration of atomic positions within the sample. The second result, indicated by the thicker curve (red), is the average result obtained from many such configurations of atomic positions. We first see that, in both cases, the spectral variations extend over a quite wide range, expressed in units of γ. This is qualitatively due to the high optical depth associated with transmission of light through the sample. Second, we observe that both the single realization and the configuration averaged cross-sections contain broad oscillations which are primarily due to diffractive scattering from the nearly opaque spherical atomic sample. The most important feature of these results is the microstructure superimposed on the broad spectral variations. Of particular interest in the context of long-lived photonic modes within the sample is the existence of the very narrow resonances apparent in the figure. These features arise from poles in the resolvent which have associated very narrow spectral widths. We point out that there is a nearly continuous spectral distribution of such poles, but that a significant fraction of them have associated narrow widths for higher atomic densities. In addition, we emphasize that the spectral locations of these poles are configuration dependent; the resonance locations are different for different spatial arrangements of the atoms in the sample.

The microstructure apparent in Figure 1 implies that there will be long-lived collective states present in any single configuration of the atomic sample. In the time domain then, we can expect evolution of light scattered from the sample to have associated relatively slowly decaying components, measured in terms of the characteristic time-scale $1/\gamma$, where γ is the natural width of the resonance transition. In Figure 2 we show just such behavior. In the figure we first point out the characteristic exponential decay of the scattered light normally expected at lower densities. The three nearly identical curves correspond to a lower density microscopic calculation ($n = 0.015$), to a solution to the diffusion equation for similar conditions, and to the decay constant corresponding to the longest lived Holstein mode. At a higher density, we see a dramatic slowing of the decay of the intensity at the longest times. This slowing occurs in coincidence with the development of the spectral microstructure of Figure 1, and corresponds to the formation of subradiant atom–field collective modes in the sample.

The time evolution of the scattered light intensity also shows systematic variations with other experimentally accessible variables. For example, we show in Figure 3 the longer time intensity decay for a spherical sample of radius $10(\lambda/2\pi)$ and several different atom densities. In Figure 3 it is apparent that for higher densities the time-scale for decay slows with increasing

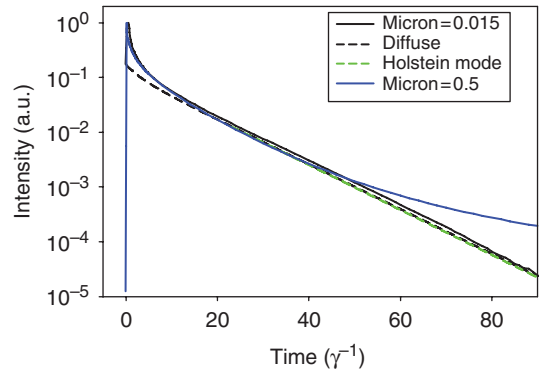

Figure 2. Comparison of the time dependence of the scattered light intensity for spherical atomic clouds of different densities, but approximately constant optical depth. Preparation of the sample is made with a temporally short pulse having a correspondingly large enough bandwidth to cover the spectral response of the system, viz. Figure 1. Microscopic results are compared with a diffusive model, and with the expected Holstein mode decay for each case. (The color version of this figure is included in the online version of the journal.)

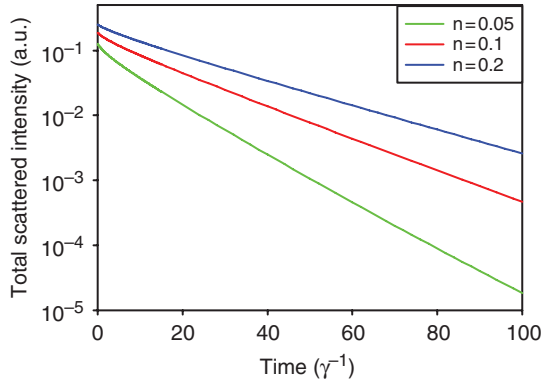

Figure 3. Time dependence of the total scattered light intensity from a uniform spherical sample of atoms of radius $10(\lambda/2\pi)$ and several different atom densities. Preparation of the sample is made with a temporally short pulse having a correspondingly large enough bandwidth to cover the spectral response of the system, viz. Figure 1. (The color version of this figure is included in the online version of the journal.)

density, this being a reflection of the combined influence of the increasing diffusive decay time and the formation at higher densities of microresonances as in Figure 1. We emphasize here that the time evolution of the afterglow of the excited atomic sample strongly depends on the conditions of excitation. For instance, the results in Figures 2 and 3 are obtained for excitation of the cloud by a very short pulse, the spectrum of which encompasses the entire manifold of excited states of the ensemble. Alternatively, we can

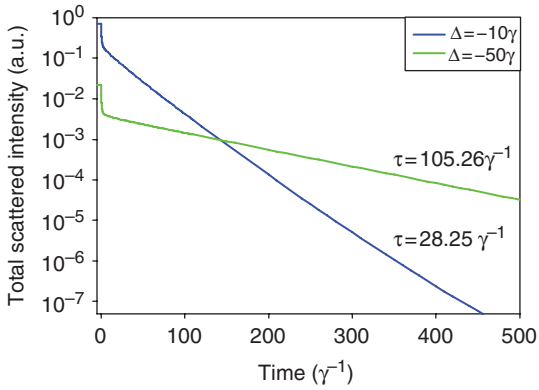

Figure 4. Time dependence of the total scattered light intensity from a uniform spherical sample of atoms for two different detunings from bare resonance. Calculation is done using the vector model. Excitation is with a temporally long, 100 γ^{-1} pulse, corresponding to a narrower pulse bandwidth than the results of Figures 2 and 3. The sample contains 1000 atoms and has an atom density $n = 0.1$. (The color version of this figure is included in the online version of the journal.)

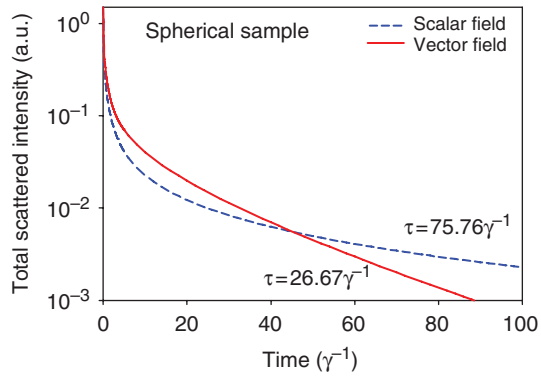

Figure 5. Comparison of vector and scalar field results for the time evolution of the total scattered light intensity in a dense medium: $n = 0.1$. Excitation is with a temporally long, 100 γ^{-1} pulse, corresponding to a narrower pulse bandwidth than the results of Figures 2 and 3. (The color version of this figure is included in the online version of the journal.)

excite the cloud with a temporally longer pulse, one which has an associated narrower spectrum. This allows us to select spectral regions with the highest density of longer-lived states.

The long time exponential decay for two different spectral detunings from resonance are shown in Figure 4. These curves correspond to excitation with a long, and thus spectrally narrow, pulse, as discussed in the previous paragraph. Shown are the associated decay constants, from which we see that the rate of decay is slower for larger detunings in this case. As discussed previously, this connects directly with the spectral distribution of collective states having different lifetimes; to be more precise, with the spectral distribution of resolvent poles with different imaginary parts. The existence of long-lived states is determined by the strong interatomic interactions, which also causes large spectral shifts of such states. To effectively generate excitation of these states with a long pulse, we must use light with its central frequency essentially shifted from the free atom resonance frequency.

To close this section, we consider the results of Figure 5. These calculations of the time evolution of the total light intensity are made for a spherical sample of density $n = 0.1$ and show the clear effects of using a more-correct vector model of the light–matter microscopic interaction in comparison with a scalar one. Although we have shown such effects to be quite negligible for lower atomic densities, for the higher density cases of importance to light trapping, light localization and random lasing, for example, the scalar approximation should not in general be made in order to obtain the most reliable results.

3. Light storage and electromagnetically induced transparency

3.1. Introduction

A second area of theoretical and experimental research interest in our group is multiple light scattering in a medium dressed with a strong control field. In this section, we first present a synopsis of our theoretical approach and some results taken from Datsyuk et al. [10]. This is followed by an overview of more recently completed initial experiments in a similar electronic Λ configuration [39]; these results indicate that, along with the forward scattered beam, the light scattered out of the coherent forward beam also propagates under conditions of electromagnetically induced transparency. Here we briefly summarize the theoretical and experimental approaches, but we refer the reader to those papers for detailed exposition of our theoretical and experimental studies, and focus here on some illustrative results.

3.2. Theoretical and experimental approaches and results

3.2.1. Theory

Light transport in a dilute medium generally performs a diffusion-type process, which in a semiclassical picture can be visualized as a forwardly propagating wave randomly scattered by atoms in a sample. In an optically dense medium this process generates a zigzag-type path consisting of either macroscopically or mesoscopically scaled segments of forwardly propagating waves. To describe such a process theoretically we solve three problems. First we determine the scattering tensor amplitude for an arbitrary elementary

incoherent scattering event. Then we describe forward propagation of the light between two successive incoherent scattering events. This is theoretically accomplished through the Green's function formalism. This function is completely described by the macroscopic susceptibility tensor of the atomic medium, which in the considered case of a cloud of ultracold atoms, under conditions of electromagnetically induced transparency (EIT), is spatially inhomogeneous and optically anisotropic (for more detail, see [10]). In spite of this inhomogeneity and anisotropy we are able to solve analytically the system of Dyson-type equations for the polarization components of the retarded Green function for the light. Knowledge of the analytical expressions for both the scattering tensor and photon Green function allows us to solve the last, and third component of this problem, which is averaging over all possible random scattering chains. This is done through the framework of the procedure of Monte Carlo simulation. Realization of this theoretical approach [10] allows us to describe the polarization, the spectral and the temporal properties of the scattered light.

One of the more important results from our earlier theoretical papers [10] is that the light scattered out of the coherent probe beam continues to propagate through multiple scattering in the medium dressed by the external control field. This means that the role of this light in the subsequent storage and retrieval of any photonic pulse has to be treated properly; that is, the coherence associated with the multiple scattering process has to be taken into account.

We have used the scheme of Figure 6 to illustrate features of this effect. In that scheme, which refers to the D_1-line of ^{87}Rb, the coupling field is applied with right-handed circular polarization to the $F=2\rightarrow F'=1$ transition. The probe mode, on the other hand, is applied in the orthogonal left-handed polarization and excites the atoms via the $F=1\rightarrow F'=1$ transition. The two fields are assumed to be in two-photon resonance. The temporal profile of the probe intensity is taken to be Gaussian with a width of 100 γ^{-1}. The pulse reaches its peak intensity at a time $t=0$. Examination of the results shown in Figure 7 shows that the light emerging from the sample has a significant extension to longer times, particularly for the Rayleigh $\sigma_+\rightarrow h_-$ scattering channel. This is a manifestation of the well known slow-light effect in the scattering channels. This effect is normally associated with the forward scattering of the probe beam, but the results of [10] clearly show that the sample dressing by the control field plays a significant role in the scattered light dynamics. Finally, we point out that the temporal beating in the scattered light intensity is a result of the spectral distortion of the incident pulse by the EIT prepared medium. In other words, the Gaussian

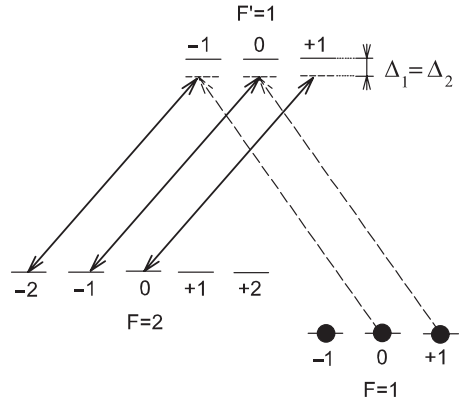

Figure 6. An example of an excitation scheme for observation of the EIT effect in the system of hyperfine and Zeeman sublevels of the D_1-line of ^{87}Rb. The coupling field is applied with right-handed circular polarization to the $F=2\rightarrow F'=1$ transition and the probe mode in the orthogonal left-handed polarization excites the atoms on the $F=1\rightarrow F'=1$ transition. The EIT effect appears for equal detunings of the coupling and probe modes from atomic resonances: $\Delta_1=\Delta_2$.

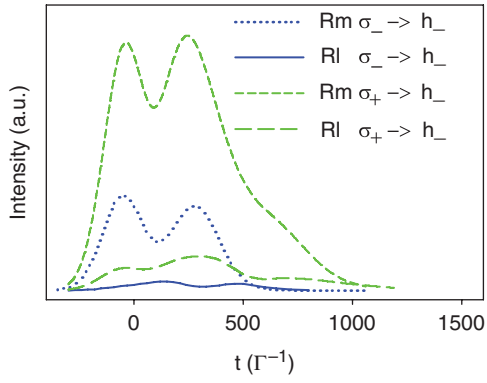

Figure 7. The intensity profiles for the portion of the light pulse scattered at 90° to the direction of the incident pulse. The curves represent the Rayleigh (Rl) channel ($F=1\rightarrow F'=1\rightarrow F=1$) and the Raman (Rm) channel ($F=1\rightarrow F'=1\rightarrow F=2$), with the input polarization state, and polarization channel of the emerging light as indicated in the caption. In all cases, the observation channel corresponds to detection of light with left-hand helicity (h_-). (The color version of this figure is included in the online version of the journal.)

spectral distribution associated with the incident pulse is transformed by the medium, and particularly by the transparency associated with the EIT effect. The spectral hole generated in the probe spectrum results in beating at the frequency associated approximately with the width of the EIT transparency.

3.2.2. *Experiment*

The experimental program focuses on ultracold atomic samples prepared and confined in a magneto optical

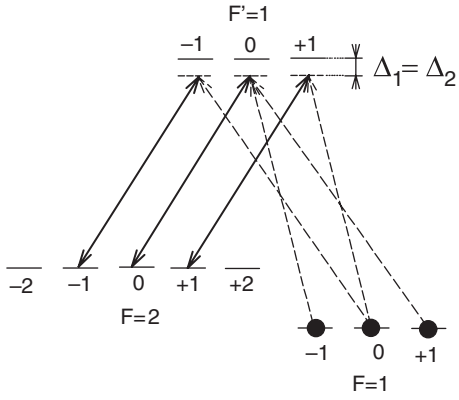

Figure 8. Experimental probe and control field excitation configuration associated with the $F=1 \rightarrow F'=1 \rightarrow F=2$ transition of the D_2 line in ^{87}Rb. The control field is indicated by the solid lines, and the probe by dashed lines. The illustration corresponds to two-photon resonance; Zeeman level light shifts ~1 MHz associated with off resonance transitions are not shown.

trap (MOT). We present here highlights of the experimental instrumentation: details are presented elsewhere [39]. The ^{87}Rb MOT is arranged in a standard vapor loaded configuration, and consists of samples of about 10^7 atoms with a Gaussian radius of 0.3 mm. The sample has an optical depth, on the $F=2 \rightarrow F'=3$ trapping transition, of about 10, while the atom sample has a typical temperature ~100 μK. These samples are of sufficient optical depth that there can be several orders of multiple scattering of light scattered out of the probe beam. The excitation configuration we have used in our initial experiments to study the dynamics of the scattered light is shown in Figure 8. In this scheme, the linearly polarized control field (z quantization axis) is tuned in the vicinity of the $F=2 \rightarrow F'=1$ transition, while the much weaker linearly polarized (x direction) probe beam is tuned near the $F=1 \rightarrow F'=1$ transition. The two lasers are characteristically tuned to be near two-photon resonance, where $\Delta_1 = \Delta_2$. We point out that this configuration is not optimal for obtaining large orders of multiple scattering. The main reason for this is that there are open decay channels to the $F=2$, $m=\pm 2$ states, in which population can be trapped for relatively long periods of time.

The basic experimental approach is shown schematically in Figure 9. In the figure, it is seen that the pump and control fields, depicted by ω_p and ω_c, respectively, propagate in approximately collinear fashion through the sample. The lasers are external cavity diode lasers, locked to saturated absorption resonances in a Rb vapor cell, and frequency tuned and switched in the conventional way with acousto optical modulators. Each laser has a long time average bandwidth on the order of 500 kHz. In these initial experiments, the two lasers are not mutually phase locked; the combined laser bandwidths then provide the ultimate limit to the characteristic ground state coherence lifetime. In the experiment, a small angle is arranged between them in order to suppress background due to the much more intense control field on top of the relatively weak probe beam intensity. Further suppression is achieved by means of a linear polarization analyzer (PA) placed directly in the path of the probe and control beams. An optical chopper is used to minimize intense MOT fluorescence signals while the sample is being loaded; the chopper trigger is used as a master switch to initiate each data cycle, minimizing the relative absolute instability of the chopper timing. The probe laser beam is launched into an optical fiber which transmits the light to a photomultiplier operating in a photon counting mode. Following amplification of the individual pulses, the signals are time sorted with up to 5 ns resolution in a multichannel scalar (MCS). The MCS also serves to accumulate and store the data for later analysis.

Under conditions of two-photon resonance, and for typical control and probe field intensities, we have found that, in our experimental conditions, it takes about 500 ns for the transmitted light to reach an approximately steady state level. With this configuration, we have been able to observe slowed transmission of the forward scattered probe beam, and also to measure so-called stopped light pulses for a range of different delay times. In these measurements, which we present elsewhere [39], the control and probe fields are turned off in an approximately adiabatic way; later reapplication of the control field to the sample generates, from the dark-state polariton, a retrieval of the forward scattered pulse. The lifetime of the regenerated pulses is quite short in the present experiment, and is limited by the mutual coherence of the ground state hyperfine levels. This in turn is determined by the relative phase instability of the control and probe fields. It is the storage and retrieval of such light pulses that provides an intriguing option for using EIT as the basis for an optical memory.

However, the primary focus of our projects is comparison of the forward scattered light with the sideways, or diffusely scattered light. To illustrate that comparison, we present in Figure 10 the transparency in the forward scattered light as a function of detuning of the weak probe beam from two-photon resonance. These data were taken for a control field Rabi frequency of 1.2 γ. From the figure, we see that there is a limited transparency in the transmitted light due to the relative sizes of the control Rabi frequency and the bandwidth due to the quite short ground state coherence time; larger control Rabi frequencies lead to nearly complete transparency [39]. The corresponding

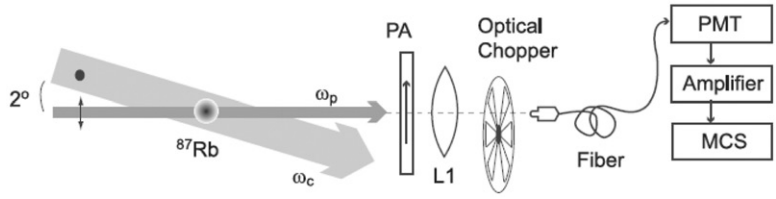

Figure 9. Schematic diagram of the time evolution of transmitted, stored, and retrieved using the level scheme of Figure 8. PA stands for polarization analyzer, PMT represents a photomultiplier tube, and MCS indicates a multichannel scalar.

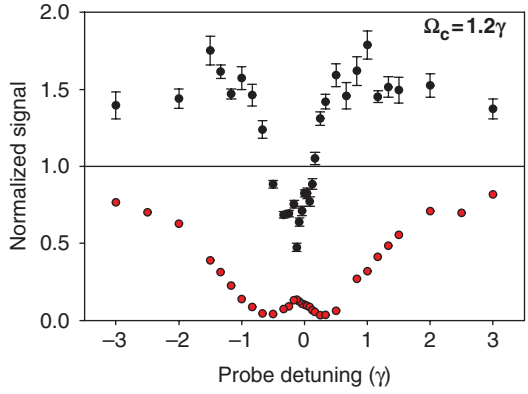

Figure 10. Comparison of forward and diffusely scattered light using the level configuration of Figure 8, and the experimental scheme of Figure 9. The lower panel (red circles) refers to transmission, while the upper panel (black circles) refers to the diffusely scattered data. The data correspond to variations of the weak probe laser frequency around two photon resonance, and to a control field Rabi frequency $\Omega_c = 0.7\ \gamma$; with reference to Figure 8, Ω_c refers to the average control Rabi frequency for the three indicated transitions. (The color version of this figure is included in the online version of the journal.)

suppression of diffusely scattered light in the vicinity of two-photon resonance is evident in the upper panel of Figure 10. Theoretical analysis of the time evolution of this scattered light suggests that it propagates with a reduced group velocity, just as the forward scattered light. Our current projects are focused towards establishing the coherence properties of the multiply scattered light through observation of the coherent backscattering cone [10].

Finally, we point out that the present arrangement is not optimum, both because of the configuration used and because of the limited scale of the ground state coherence; further research is underway to extend this scale, and the amount of multiple scattering, in order to explore the role of coherent multiple scattering on the ultimate lifetime of light storage in ultracold and dense atomic gases. Further details of these experiments, including the effects of the control dressing field on the propagation of the light scattered from the probe pulse, are presented elsewhere [39].

4. Summary

In this paper we have briefly summarized some aspects of our theoretical and experimental studies of light storage in dense and ultracold atomic gases. The two approaches we use have as a common theme the role of coherent multiple scattering in such media. For lower atomic densities, multiple scattering may serve as a limiting factor in photon storage time. There also is the intriguing possibility that a new type of quasiparticle, a diffuse dark state polariton, may be formed. Experiments in that direction are underway. For greater atomic densities, recurrent multiple scattering may lead to formation of long-lived subradiant modes; these modes may serve in themselves as a means to store photonic information. Control of these modes may be achieved by manipulating dynamically the optical depth of the atomic media. One way to achieve this is through rapid control of the light shift of the involved atomic resonance levels.

Acknowledgements

This work was supported by RFBR (Grant Nos. 10-02-00103 and 08-02-91355) and by the National Science Foundation (Grant No. NSF-PHY-0654226).

References

[1] Nielsen, M.A.; Chuang, I.L. *Quantum Computation and Quantum Information*; Cambridge University Press: Cambridge, UK, 2000; p 517.
[2] Briegel, H.-J.; Dur, W.; Cirac, J.I.; Zoller, P. *Phys. Rev. Lett*. **1998,** *81,* 5932–5935.
[3] Duan, L.-M.; Lukin, M.D.; Cirac, J.I.; Zoller, P. *Nature* **2001,** *414,* 413–418.
[4] Metcalf, H.J.; van der Straten, P. *Laser Cooling and Trapping*; Springer-Verlag: New York, 1999.

[5] Grimm, R.; Weidemuller, M.; Ovchinnokov, Y. *Adv. At. Mol. Opt. Phys.* **2000,** *42,* 95–170.

[6] Lukin, M.D. *Rev. Mod. Phys.* **2003,** *75,* 457–472.

[7] Lukin, M.D.; Imamoglu, A. *Nature* **2001,** *413,* 273–276.

[8] Chaneliere, T.; Matsukevich, D.N.; Jenkins, S.D.; Lan, S.-Y.; Kennedy, T.A.B.; Kuzmich, A. *Nature* **2005,** *438,* 833–836.

[9] Matsukevich, D.N.; Kuzmich, A. *Science* **2004,** *306,* 663–666.

[10] Datsyuk, V.M.; Sokolov, I.M.; Kupriyanov, D.V.; Havey, M.D. *Phys. Rev. A* **2006,** *74,* 043812, *Phys. Rev. A* **2008**, *77*, 033823.

[11] Akkermans, E.; Montambaux, G. *Mesoscopic Physics of Electrons and Photons*; Cambridge University Press: Cambridge, UK, 2007.

[12] Labeyrie, G.; de Thomasi, F.; Bernard, J.-C.; Muller, C.A.; Miniatura, C.; Kaiser, R. *Phys. Rev. Lett.* **1999,** *83,* 5266–5269.

[13] Bidel, Y.; Klappauf, B.; Bernard, J.C.; Delande, D.; Labeyrie, G.; Miniatura, C.; Wilkowski, D.; Kaiser, R. *Phys. Rev. Lett.* **2002,** *88,* 203902-1.

[14] Kupriyanov, D.V.; Sokolov, I.M.; Larionov, N.V.; Kulatunga, P.; Sukenik, C.I.; Havey, M.D. *Phys. Rev. A* **2004,** *69,* 033801.

[15] Balik, S.; Kulatunga, P.; Sukenik, C.I.; Havey, M.D.; Kupriyanov, D.V.; Sokolov, I.M. *J. Mod. Opt.* **2005,** *52,* 2269–2278.

[16] Labeyrie, G.; Miniatura, C.; Kaiser, R. *Phys. Rev. A* **2001,** *64,* 033402.

[17] Labeyrie, G.; Miniatura, C.; Muller, C.A.; Sigwarth, O.; Delande, D.; Kaiser, R. *Phys. Rev. Lett.* **2002,** *89,* 163901.

[18] Müller, C.A.; Jonckheere, T.; Miniatura, C.; Delande, D. *Phys. Rev. A* **2001,** *64,* 053804.

[19] Kupriyanov, D.V.; Sokolov, I.M.; Havey, M.D. *Opt. Commun.* **2004,** *243,* 165–173.

[20] Havey, M.D. *Contemp. Phys.* **2009,** *50,* 587–599.

[21] Kupriyanov, D.V.; Sokolov, I.M.; Sukenik, C.I.; Havey, M.D. *Laser Phys. Lett.* **2006,** *3,* 223–243.

[22] Labeyrie, G. *Mod. Phys. Lett.* **2008,** *B22,* 73–79.

[23] Anderson, P.W. *Phys. Rev.* **1958,** *109,* 1492–1505, *Phil. Mag.* **1985**, *52*, 505–509; Abrahams, E.; Anderson, P.W.; Licciardello, D.C.; Ramakrishnan, T.V. *Phys. Rev. Lett.* **1979,** *42,* 673–676.

[24] Sheng, P. *Introduction to Wave Scattering, Localization, and Mesoscopic Phenomena*; Academic Press: San Diego, 1995.

[25] Wiersma, D.S.; Bartolini, P.; Lagendijk, A.; Righini, R. *Nature* **1997,** *390,* 671–673.

[26] Storzer, M.; Gross, P.; Aegerter, C.M.; Maret, G. *Phys. Rev. Lett.* **2006,** *96,* 063904.

[27] Storzer, M.; Aegerter, C.M.; Maret, G. *Phys. Rev. E* **2006,** *73,* 065602(R).

[28] Guerin, W.; Michaud, F.; Kaiser, R. *Phys. Rev. Lett.* **2008,** *101,* 093002.

[29] Froufe-Perez, L.S.; Guerin, W.; Carminati, R.; Kaiser, R. *Phys. Rev. Lett.* **2009,** *102,* 173903.

[30] Scully, M.O. *Phys. Rev. Lett.* **2009,** *102,* 143601.

[31] Svidzinsky, A.A.; Chang, J.; Scully, M.O. *Phys. Rev. Lett.* **2008,** *100,* 160504.

[32] Bienaime, T.; Bux, S.; Lucioni, E.; Courteille, Ph.W.; Piovella, N.; Kaiser, R. *Phys. Rev. Lett.* **2010,** *104,* 183602.

[33] Courteille, Ph.W.; Bux, S.; Lucioni, E.; Lauber, K.; Bienaime, T.; Kaiser, R.; Piovella, N. *Eur. Phys. J. D* **2010,** *58,* 69–74.

[34] Kupriyanov, D.V.; Sokolov, I.M.; Kupriyanova, M.D.; Havey, M.D. *Phys. Rev. A* **2009,** *79,* 053405.

[35] Beresteskii, V.B.; Lifshits, E.M.; Pitaevskii, L.P. *Course of Theoretical Physics: Quantum Electrodynamics*; Pergamon Press: Oxford, UK, 1981.

[36] Hutchinson, D.A.; Hameka, H.F. *J. Chem. Phys.* **1964,** *41,* 2006–2011.

[37] Rusek, N.; Mostowski, J.; Orlowski, A. *Phys. Rev. A* **2000,** *61,* 022704; Pinheiro, F.A.; Rusek, M.; Orlowski, A.; van Tiggelen, B.A. *Phys. Rev. E* **2004,** *69,* 026605.

[38] Akkermans, E.; Gero, A.; Kaiser, R. *Phys. Rev. Lett.* **2008,** *101,* 103602.

[39] Olave, R.G.; Win, A.L.; Havey, M.D.; Sokolov, I.M.; Kupriyanov, D.V. To be submitted for publication, 2010.